Tuning branching in ceria nanocrystals and nanocrystal-based aerogels

Taisiia Berestok,[1,3] Pablo Guardia,[1,2] Javier Blanco,[3] , Luis López-Conesa,[3] Sònia Estradé,[3] Maria Ibáñez[4], Raquel Nafria,[1] Jonathan de Roo,[5,6] Zhishan Luo,[1] Jose C. Martins,[6] Maksym V. Kovalenko,[4,7] Stephanie L. Brock,[8] Francesca Peiró,[3,*] and Andreu Cabot[1,9,*]

1) Catalonia Institute for Energy Research – IREC, 08930 Sant Adrià de Besòs, Barcelona, Spain
2) Centre de Tecnologia Química de Catalunya and Universitat Rovira i Virgili, 43007 Tarragona, Spain
3) LENS-MIND, Departament d'Enginyeries i Electrònica i Institut de Nanociència i Nanotecnologia (In2UB), Universitat de Barcelona, 08028, Barcelona, Spain
4) Institute of Inorganic Chemistry, Department of Chemistry and Applied Biosciences, ETH Zürich, CH-8093, Switzerland
5) Department of Inorganic and Physical Chemistry, Ghent University, B-9000 Ghent, Belgium
6) Department of Organic and Marcromolecular Chemistry, Ghent University, B-9000 Ghent, Belgium
7) Empa-Swiss Federal Laboratories for Materials Science and Technology, Dübendorf, CH-8600, Switzerland
8) Department of Chemistry, Wayne State University, Detroit, Michigan 48202, United States
9) ICREA, Pg. Lluís Companys 23, 08010 Barcelona, Spain

ABSTRACT

Branched nanocrystals (NCs) enable high atomic surface exposure within a crystalline network that provides optimized transport properties. Herein we report on the colloidal synthesis of branched ceria NCs by means of a ligand-mediated overgrowth mechanism. In particular, the differential coverage of oleic acid as X-type ligand at ceria facet with different atomic density, atomic coordination deficiency and oxygen vacancy density, results in a preferential growth in the [111] direction and thus in the formation of ceria octapods. Alcohols, through and esterification alcoholysis reaction, promote faster growth rates that translate into nanostructures with higher geometrical complexity, increasing the branch aspect ratio and triggering the formation of side branches. The presence of water on the other hand resulted in a significant reduction of the growth rate, decreasing the reaction yield and eliminating side branching, which we associate to a displacement of the alcoholysis reaction. Overall, adjusting the amounts of each chemical, well-defined branched ceria NCs with tuned number, thickness and length of the branches and with overall size ranging from 5 to 45 nm could be produced. We further demonstrate such branched ceria NCs to provide higher surface areas and related oxygen storage capacities (OSC) than quasi-spherical NCs obtained in the presence of only oleylamine.

Keywords: Ceria, nanoparticle, branching, nanocrystal, catalysis, colloidal, shape control, tomography, oxygen storage capacity.

INTRODUCTION

Branching enables to significantly increase the surface-to-volume ratio of nanocrystals (NCs).[1-4] At the same time, compared with NCs having spherical or regular polyhedral geometries, the use of branched NCs as building blocks to produce macroscopic nanomaterials improves transport properties and provides higher levels of porosity by preventing close-packed aggregation.[5,6] Branching therefore allows a higher extent of interaction with the media while simultaneously facilitating charge carrier injection and extraction, characteristics that are particularly valuable in the fields of catalysis, sensing and in some biomedical applications.[7-10] Besides, branched nanostructures may show additional advantages such as higher magnetic anisotropy in magnetic NCs and improved surface enhanced Raman spectroscopy enhancement factors in plasmonic NCs.[11,12] Branched NCs are also easier to manipulate, purify or recuperate than unbranched NCs with equivalent surface areas.

Branching is especially interesting in the field of catalysis, where it provides higher atomic surface exposure and thus a more efficient material utilization. The asymmetric character of branches may also deliver particularly favorable facets and very large densities of edges and corners that offer highly reactive sites.[8,25,31] A particularly interesting material in this field is ceria. Ceria has become one of the most technologically important rare earth oxides, being widely used in three way catalysts, gas sensors and solid oxide fuel cells. Ceria is also used in biomedical applications to protect cells from radiation damages and oxidative stress.[32-35] As a result of its multi-valence and the positive Ce^{4+}/Ce^{3+} reduction potential, ceria contains a mixture of Ce^{3+} and Ce^{4+} oxidation states which confers outstanding capabilities to store, release and transport oxygen and oxygen vacancies, especially when nanostructured.[34,36-38] In all the applications that involve interaction with the media, ceria performance does not only depend on the crystal domain size but also on the facets exposed to the environment.[39-42] For instance, it has been established that {100} and {110} facets have lower activation energy for the formation of oxygen vacancies than {111} facets.[43,44] This translates into higher catalytic activities for a set of oxidation reactions of nanorods displaying {100} and {110} when compared with polyhedral NCs with {111} facets.[45-50,51-54] Several protocols to produce ceria NCs with controlled morphologies, including are already available. [55,56 57,585960 56,596056 6162] However, a strategy or mechanism to control branching in such a technologically important material is yet to be reported.

Branching can be induced by several mechanisms, including template-directed growth, selective etching, twinning, crystal splitting, polymorphic or heterogeneous seeded growth, ligand-mediated overgrowth and NC aggregation-based growth.[13-16] The template-directed growth makes use of a scaffold to direct the growth of the targeted material, which grows within or around it.[17,18] Among them, the overgrowth mechanism is the most versatile and simplest strategy to produce branched nanostructures as already demonstrated for a number of systems.[25-27]

Overgrowth mechanisms are generally considered as kinetically controlled. Thus, reactants and reaction conditions are selected so ions add and react to the NC much faster than they can move through the surface.[16,24] In these conditions, the NC geometry is determined by the growth rates in each crystallographic direction, which depend on the accessibility and reactivity of each facet. These parameters, and thus the NC geometry, can be manipulated through the use of facet-selective surface ligands. This

Here we describe a ligand-mediated overgrowth strategy to produce ceria NCs with tuned branching. By carefully adjusting the synthetic parameters and particularly the amount and type of ligands, branched NCs with different arm thickness and multi-branched structures originated from side-branching can be produced. We

further demonstrate the possibility to transfer these nanostructures to polar solvents and to produce NC-based hydro- and aerogels. Additionally we measure the surface area and oxygen storage capacity of the ceria NCs with different geometries.

Experimental section

Chemicals: Cerium (III) nitrate hexahydrate ($Ce(NO_3)_3{\cdot}6H_2O$, 99%), oleic acid (OAc, $C_{18}H_{34}O_2$, 90%), 1-octadecene (ODE, $C_{18}H_{36}$, 90%), oleylamine (OAm, $C_{18}H_{37}N$, 70%), 1,2-decanediol (1,2-DDOL, $C_{10}H_{22}O_2$, 90%), 1,12-dodecanediol (1,12-DDDOL, $C_{12}H_{26}O_2$, 99%), 1,2-hexadecanediol (1,2-HDDOL, $C_{16}H_{34}O_2$, 90%) L-Glutamine (GIn, $C_5H_{10}N_2O_3$, ≥99%), trifluoroacetic acid (TFA, $C_2HF_3O_2$, 99%), N,N-dimethylformamide (DMF, C_3H_7NO, 99.8%) and propylene oxide (PO, C_3H_6O, ≥99.5%) were purchase from Sigma-Aldrich. 1-Dodecanol (1-DDOL, $C_{12}H_{26}O$, 98 %) was purchased from Acros. Toluene, chloroform, and acetone were of analytical grade and were purchased from Panreac. OAm was purified by vacuum distillation. All other reagents were used as received without further purification. All experiments were carried out in 25 mL three-neck round-bottom flasks equipped with a condenser connected to a standard Schlenk line. Air and moisture-sensitive chemicals were handled and stored under inert atmosphere.

Quasi-spherical CeO_2 NCs: In a 25 mL three neck flask and under magnetic stirring, 0.434 g (1 mmol) of cerium (III) nitrate, with 2 mL (6 mmol) of OAm were mixed in 4 mL of ODE. After degassing for 30 minutes at 80 °C, a brown colour solution was formed. The mixture was then heated under argon flow up to 300 °C at a rate of 15 °C/min. During heating up, at around 200 °C, the solution became turbid and started to change color to dark brown. The mixture was allowed to react at 300 °C for 60 minutes before cooling to room temperature. During the cooling down, at around 160 °C, 2 mL of toluene were injected. NCs were finally collected by precipitation, adding 25 mL of acetone and centrifuging the solution at 6500 rpm for 6 minutes. The supernatant was discarded and the black precipitate was dispersed in 5 mL of chloroform. This precipitation-redispersion procedure was repeated four times to remove excess of surfactants.

Branched CeO_2 NCs: To synthesize branched ceria NCs the protocol described above was used, but including OAc and eventually alcohols to the initial solution of cerium (III) nitrate, OAm and ODE. In particular, we added 2 mL of OAc (6 mmol) and selected amounts of alcohols (0, 1.25, 2, 2.2 and 2.5 mmols) to produced branched NCs with different geometries. Detailed synthesis parameters for each sample are displayed in Table S1.

Ligand exchange: Ligand exchange processes were carried out at ambient atmosphere. 7 mg of GIn was dissolved in 1 mL DMF followed by the addition of 1 mL of NCs (5 mg/mL) solution in hexane. After shaking of the obtained two-phase solution, 20 μL of TFA was added. The mixture was stirred until the transferring of NCs from the upper to the bottom part took place. NCs were separated from the supernatant followed by the addition of fresh hexane/acetone mixture with further centrifuging. NPs were cleaned several times with DMF as a solvent and mixture of hexane/acetone as an antisolvent. The obtained NCs could be redispersed in polar solvents, including water.

Hydrogel and aerogel formation: Gelation procedure was performed in air. In a typical experiment, the amino-acid functionalized CeO_2 NCs (20 mg/mL) were redispersed in 2 mL of DMF to form a stable solution followed by the addition of 1 mL aliquots of MQ-water. The mixture was sonicated for approximately 15 min. To induce gelation, 2 mL of propylene oxide (PO) were added and the solution was stored undisturbed until gelation took place. The gelation process occurred within 24 h and the obtained gels were aged for several days. Then the gel

solvent was exchanged with 5 mL aliquots of acetone without disturbing the porous structure of the gel. The exchanging of the solvent was repeated for at least 6 times. After replacing the solvent by acetone the resulted alco-gel together with additional acetone was loaded into chamber of supercritical point drier. The chamber of the equipment was sealed followed by slow flushing with liquid CO_2 using the metering pump. After overnight storage undisturbed, the liquid CO_2 inside of the chamber was half-drained and filled with fresh one. This procedure was repeated for at least 6 times in one-hour intervals in order to replace the acetone with liquid CO_2. After exchanging the solvent by CO_2 was completed the chamber was heated to 39 ^oC leading to increasing of the pressure to 75-80 bars. The sample was kept under these conditions for 1 h followed by releasing the pressure while keeping the temperature constant.

Structural and chemical characterization: Transmission electron microscopy (TEM) characterization was carried out using a ZEISS LIBRA 120, operating at 120 kV. High resolution TEM (HRTEM) studies were performed in a JEOL 2010F TEM operating at an accelerating voltage of 200 kV. Samples were prepared by drop casting a diluted solution of ceria NCs onto a carbon coated cooper grid (200 mesh). Images were analyzed with the Gatan Digital Micrograph software. X-ray power diffraction (XRD) analyses were carried out on a Bruker AXS D8 ADVANCE X-ray diffractometer with Ni-filtered (2 μm thickness) Cu Kα1 radiation (λ = 1.5406 Å). Samples were drop casted (200-500 μL at a concentration of about 3 mg/mL) onto a zero-signal silicon wafer. UV-vis absorption spectra were recorded on a PerkinElmer LAMBDA 950 UV−vis spectrophotometer. Samples were prepared by diluting 100 μL in 3 mL of chloroform inside a 10 mm path length quartz cuvette. FTIR spectroscopy investigations were carried out using a PerkinElmer FT-IR 2000 spectrophotometer. Spectra were recorded form 500 cm^{-1} to 4000 cm^{-1}. Thermogravimetric analyses (TGA) were carried out on a PerkinElmer Diamond TG/DTA instrument. For TGA analysis, samples were thoroughly dried and 20 mg of the dried powder was loaded into a ceramic pan. Measurements were carried out in an air atmosphere from ambient temperature to 700 °C at a heating rate of 5 °C/min. Nuclear magnetic resonance (NMR) measurements were recorded on a Bruker Avance III Spectrometer operating at a ^1H frequency of 500.13 MHz and equipped with a BBI-Z probe. The sample temperature was set to 298.2 K.

Catalyst preparation and characterization: Samples were annealed at 400 °C for 4 h under air atmosphere using a heating ramp of 2 °C /min. The specific surface area and pore size of the materials was determined by N_2 adsorption at 77 K using a Tristar II 3020 Micromeritics system. Specific areas were calculated using Brunauer-Emmet-Teller (BET) method, from the analysis of the adsorption at P/P_o= 0.999. Hydrogen temperature-programmed reduction (TPR) was performed on annealed samples using a Micromeritics AutoChem HP 2950 chemisorption analyzer. Briefly, 50 mg of sample was pretreated at 90 °C for 15 min under flowing He (50 mL/min). After cooling to room temperature, the samples were reduced in a flow of 12 vol % H_2/Ar (50 mL/min), and temperature was linearly increased at a rate of 10 °C/min up to 930 °C. Oxygen storage capacities (OSC) of annealed samples were investigated by carrying out TGA experiments using a Sensys evo DSC instrument (Setaram) equipped with 3D thermal flow sensor. The sample was loaded into twin fixed-bed reactors, with one of the reactors serving as the reference. Each sample was treated in an Ar atmosphere for 1 h at 553 K to eliminate the adsorbed water, followed by heating at a constant rate (5 K/min) up to 673 K. At this temperature the materials were exposed to a flow of 12 vol % H_2/Ar (50 mL/min) and kept at this temperature for 1 h. The observed weight loss was associated to the removal of oxygen by H_2 to form water. Thus from the weight loss an oxygen storage capacity at that temperature was calculated.

RESULTS AND DISCUSSION

CeO_2 NCs were produced by the decomposition of cerium nitrate in the presence of OAm at temperatures up to 300 °C. Upon addition of the cerium salt to the ODE solution containing OAm and heating to 80 °C, a cerium-OAm complex is formed.[63] This complex started to decompose at around 200 °C to produce quasi-spherical CeO_2 NCs with a ca. 90% material yield (Figure 1a). In pure ODE, without OAm, cerium nitrate could not be dissolved and when attempting to react it at high temperature (300 °C), no CeO_2 NCs could be recovered.

Cerium nitrate was soluble at moderate temperatures (~100 °C) in the presence of OAc, probably forming cerium oleate. However, in the sole presence OAc, without OAm, no CeO_2 NCs were produced due to the chemical dissolution of ceria by OAc. The presence of equivalent amounts of OAc and OAm, to prevent NC dissolution, resulted in the growth of ceria NCs but with significantly differences when compared with the growth under only OAm. In the presence of OAc, a 3-fold decrease of the number of nucleation events and a 2-fold reduction of the final material yield of the reaction was obtained. Additionally, NCs with branched geometries were produced (Figure 1b).

With respect to the reaction mixture containing Oam and OAc, the incorporation of alcohols strongly increased the material yield, to ca. 80% and accelerated the NC growth, while resulting in a similar number of NCs. In the presence of alcohols systematically larger ceria NCs containing additional and higher aspect ratio branches (Figures 1c and S3b) were produced. Relatively large concentrations of alcohols (*e.g.* 2.5 mmol 1,2-HDDOL) resulted in hyperbranched NCs with an overall cubic shape (Figure 1f).

HRTEM and electron diffraction analysis showed all branched NCs to be single crystal and branches to grow along the [111] crystallographic directions (Figures 1 i-l). In contrast, aggregates of quasi-spherical NCs provided polycrystalline SAED pattern (Figures 1 g-h). XRD patterns (Figure S6) displayed the reflections of the CeO_2 fluorite structure (space group = Fm3m, JCPDS card No 34-0394) with lattice parameter a = 0.5412 nm. The crystal domain size calculated from the broadening of the XRD reflections using Scherer equation matched well with the NC size obtained from TEM (Table S2), including clear differences on the crystal domain size in different crystallographic directions.

HAAF-STEM tomography analysis revealed the NCs produced in the presence of OAc, but no alcohols, to have an octapod-like geometry (Figure Sx). Additionally, a more detailed view of the octapods morphology was obtained through atomic simulations, (Figure 2). Modeling was conducted on NCs oriented along the [100] zone-axis, since HRTEM and FFT analyses showed this to be the most common for octapods (Figure 1i and 3 and S8). Simulations were carried out by dividing an octapod structure in a central body (spherical, zone-axis [001], Figure 3c) and a set of arms (hexagonal truncated pyramids) pointing in the [111] directions corresponding to the corners of a cube centered in the origin of the supercell. Simulation results were in good agreement with experimental HRTEM images, where the distribution of the NC atomic columns was well reproduced (Figures 3a and S9). Regarding to the tomographic results, the model projections in [001] and [110] orientations also fitted well the experimental images (Figure S8), even if the high degree symmetry of the regular atomic model proposed did not take into account some of the defects observed in the experimental images, such as the bifurcations in the arms of the octapod (Figure S14).

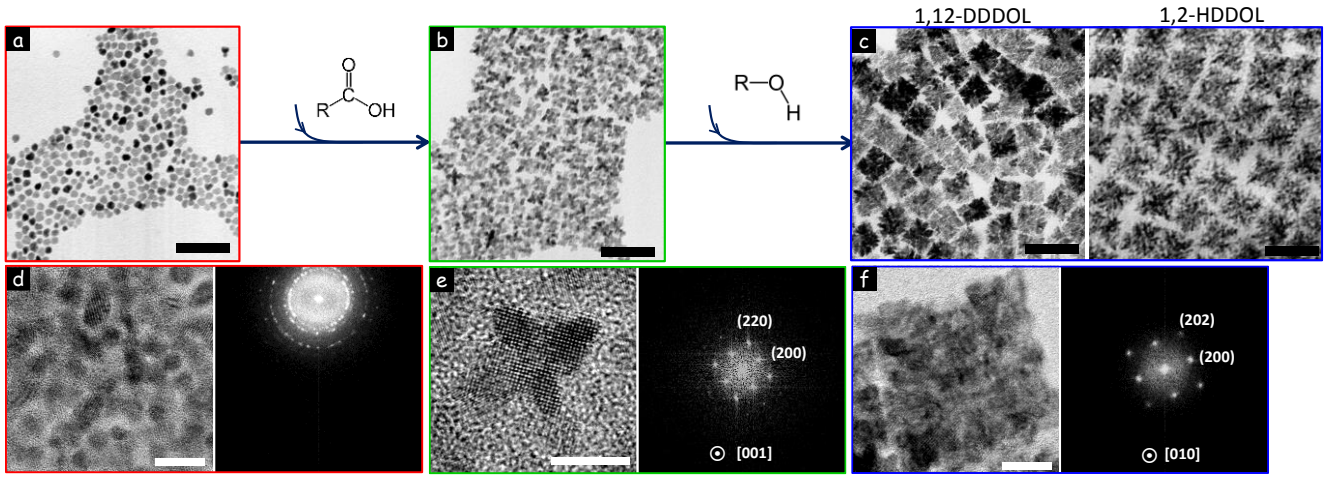

Figure 1. Representative TEM micrograph of ceria NCs obtained in the presence of different ligands: a) Quasi-spherical NCs obtained in the presence of OAm; b) branched ceria NCs produced with the additional incorporation of OAc; c) side-branched ceria NCs obtained in the presence of 1,12-DDDOL and 1,2-HDDOL. Details for the syntheses are summarized in Table S1. d-f) High-resolution TEM images and corresponding fast Fourier transform of quasi-spherical (d), branched (e) and hyperbranched (f) NCs. Scale bar of TEM images = 50 nm. Scale bar of HRTEM images = 5 nm.

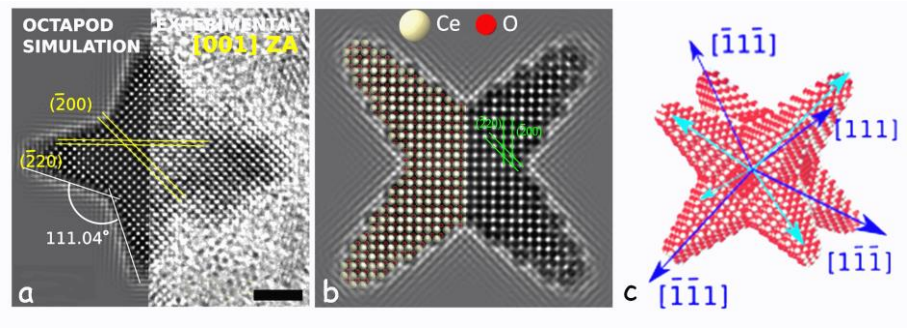

Figure 2. a) Comparision between the HRTEM simulated (left) and the experimental (bright) images of a ceria octapod. b) Superposition of the atomic model shown with zone axis [001] and the simulated image. c) 3D model of a CeO_2 octapod. In cyan the complementary directions to the ones shown in blue for the family (111)).

The formation of ceria octapods in the presence of OAc is consistent with previous reports demonstrating the synthesis of octapods of a range of metals and metal oxides. Octapod formation has been associated either to a selective etching of [100] facets or the selective overgrowth in the [111] crystallographic direction. The latter case has been hypothesized to be triggered either by the preferential interaction of OAc with [100] facets blocking monomer delivery and thus hindering their growth or quite the opposite by its preferential interaction with the [111] facets, providing monomer (oleate) and thus accelerating growth in this direction.[6465] However, scarce evidences to support these hypothesis have been given.

On the other hand, some previous works also reported the formation of complex CeO_2 nanostructures through the oriented attachment of cubic NCs mediated by the preferential binding of OAc at [100] facets. While it is not always straightforward to discern the mechanism involved in the formation of particular branched NCs, a main

differential characteristic of aggregation growth when compared with atomic-addition is that aggregation growth takes place within a solution containing a population of small NCs which decreases as being added to larger structures. Eventually, when all small NCs have been consumed, growth stops.

To elucidate the growth mechanism of the branched structures here described, aliquots at different reaction times were withdrew and analyzed (Figure 2). Interesting, NCs produced at low reaction times already showed a branched geometry and no population of smaller NCs was observed. As reaction time increased the size of all NCs in the ensemble simultaneously increased while their geometry was preserved. This observation clearly pointed out at the formation of branched NCs through atomic addition and not through a selective etching or NC aggregation mechanism.

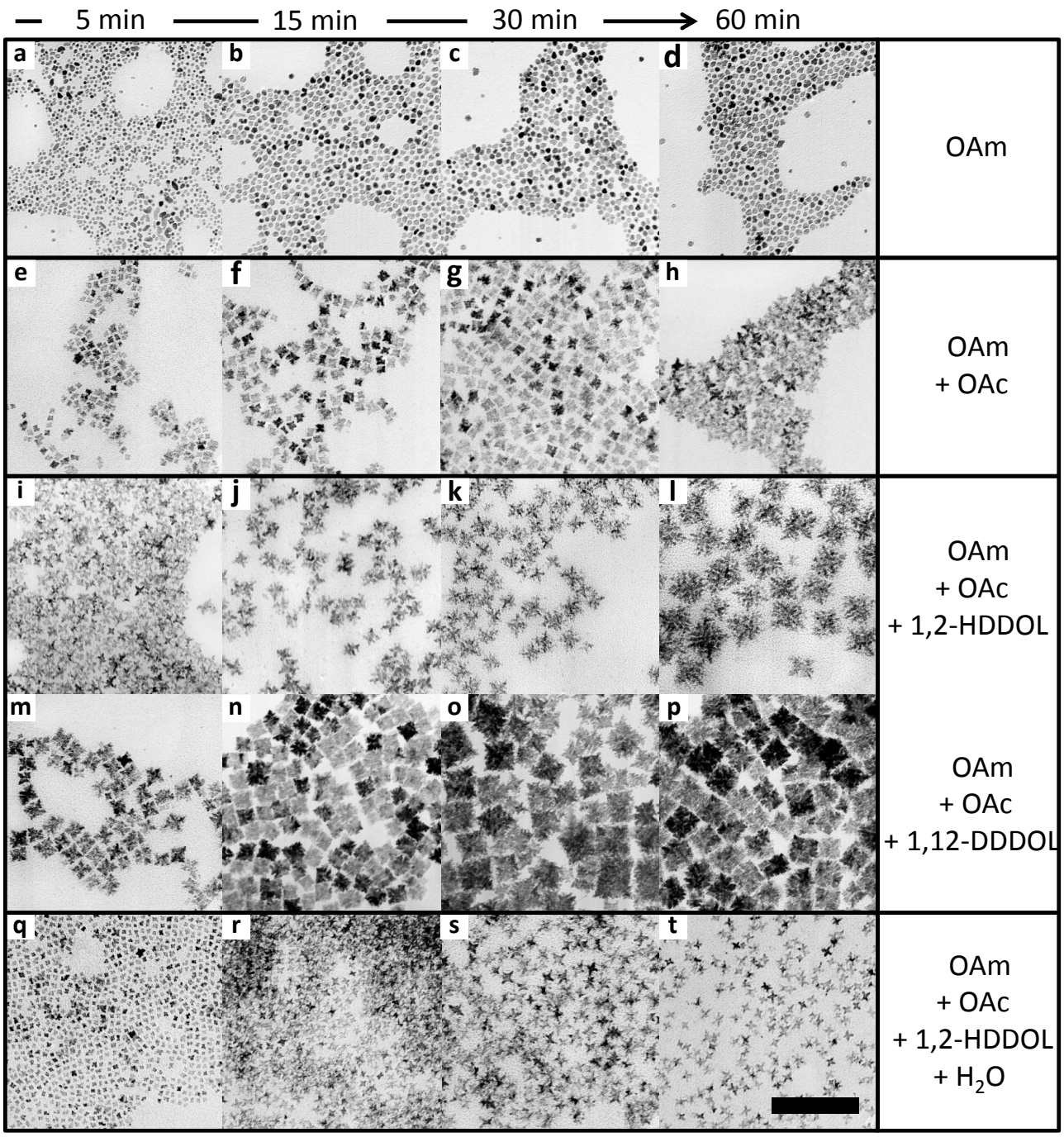

Figure 3. Representative TEM micrographs of the ceria NCs obtained at different reaction times (5, 15, 30 and 60 min): a-d) in the presence of only OAm; e-h) adding OAc; i-l) adding OAc and 1,2-HDDOL; m-p) adding OAc and 1,12-DDDOL; q-t) adding OAc, 1,2-HDDOL and MQ-water. Experimental details for each image are summarized in Table S1. All images were taken at the same magnification. Scale bar = 50 nm.

To determine the specific OAc effect, either to block monomer delivery to the (100) facets favoring in this way the preferential growth of the [111] direction or to preferentially deliver monomer to the (111) facets in an OAm passivated crystal, the NC surface chemistry was examined by NMR. NMR analysis confirmed the presence of

OAc in the surface of octapods and hyperbranched NCs. In the ^{1}H NMR spectrum of purified hyperbranched NCs, the ligand resonances are broadened (Figure ??). The severe line broadening is in line with the large size and the many chemical environments of such nanostructures. However, it also impedes the determination of the ligand's identity. Therefore, we added trifluoroacetic acid to the NCs to cleave the ligands from the NC surface. As a result, the NCs precipitated and we analyzed the supernatant. Figure ??? clearly shows a set of resonances that agrees with the fingerprint of OAc. No evidences of the presence of OAm and alcohol at the NC surface could be obtained by NMR. Thus we conclude that OAc was the sole ligand on the surface of branched ceria NCs. To further underscore this point and determine the type of binding, we added 10-undecenoic acid to a purified NC dispersion and the broadened resonances of 10-undecenoic acid was observed (Figure ???), indicating an X-for-X ligand exchange at the NCs surface.(ref. De Roo, J., De Keukeleere, K., Hens, Z. & Van Driessche, I. From ligands to binding motifs and beyond; the enhanced versatility of nanocrystal surfaces. *Dalton Trans* **45**, 13277-13283, doi:10.1039/c6dt02410f (2016)). Thus we had to conclude OAc triggers the formation of branches by selectively bidning, as an X-type ligand to the majoritary NC facets living the (111) facets as the less protected.

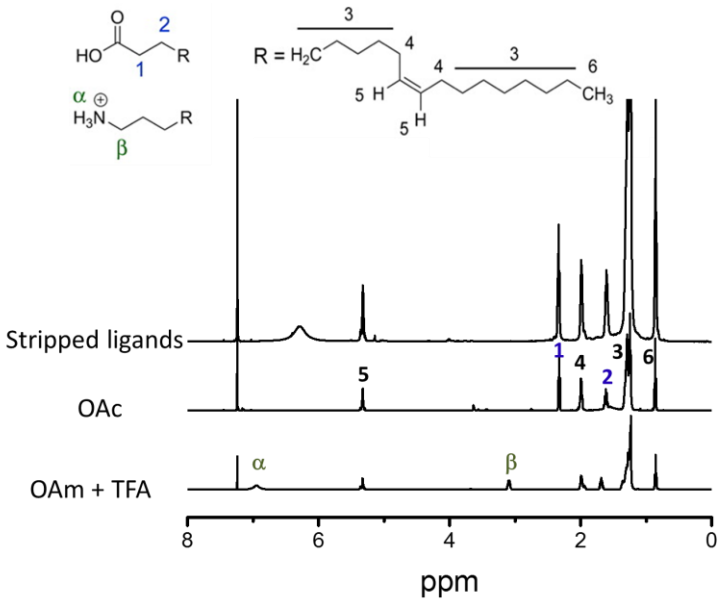

Figure 4. 1H NMR spectrum of stripped lignads from hyperbranched ceria NCs and reference spectra of Oac and Oam.

Semiquantitative NMR analysis to see if amount of OAc matches surface area?

Three intrinsic properties of the ceria crystal structure may explain the lower coverage of the (111) facets by OAc. First, the (111) is the most compact surface, which may prevent a close packed structure of relatively bulky OAc. Additionally, (111) facets have surface atoms with the lowest coordination deficiency thus difficulting ligand bonding. Moreover, this facet is the one showing larger oxygen vacancy formation energies and thus having the lowest density of such a defect which is required to compensate charge when OAc coordinates as an X-type ligand.

On the other hand, alcohols have been used as reducing, reactant and stabilizing agents in the synthesis of a plethora of oxide and metallic NCs.[66-69] In the present case, the absence of their fingerprint in the NMR pattern and the increased growth rates triggered point at their role as reactants in an esterification alcoholysis reaction of the oleate monomer.[70,71] In parallel, alcohols may consume part of the free acid via the esterification reaction reducing the ceria dissolution rate. This overall modification of the growth kinetics directed the formation of sharper branches (add ref: Y. Chen, M. Kim, G. Lian, M. B. Johnson, X. Peng, J. Am. Chem. Soc. 2005, 127, 13331) and triggered the creation of higher amounts of defects which acted as nucleation sites for new side branches, thus resulting in hyperbranched structures.[21] At high concentrations of alcohol groups, very fast rates and nucleation sites densities were obtained, resembling a dendritic growth.

Water is a byproduct of the esterification reaction that could influence the reaction kinetics. To elucidate this influence, controlled amounts of MQ-water were injected to the reaction mixture. The presence of MQ-water had a contrary effect to that of alcohols, reducing the growth rate and yield and preventing side-branching. As shown in figure 5, at a constant amount of an alcohol (*i.e.* 2.5 mmols of 1,2-HDDOL), increasing the amount of added MQ-water (0, 1 and 1.5 mL) induced a morphology transformation from hyper-branched to octapod structures (Figure S3g-i). Additionally, the NCs obtained in the presence of water were systematically smaller than those produced under the same conditions but in its absence. We believe that the presence of water slowed down the reaction of alcohols and fatty acids and thus the formation of an ester by a displacement of the esterification reaction.

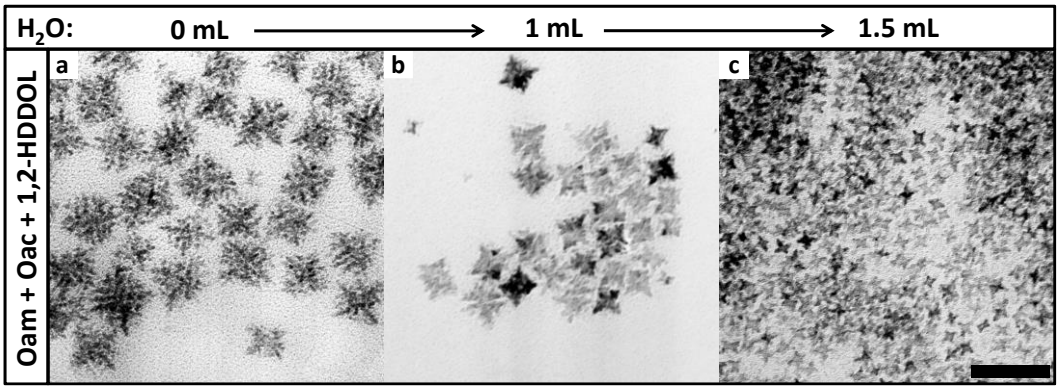

Figure 5. Representative TEM micrograph of ceria NCs produced in the presence of different amounts of water while maintaining constant all other conditions. Notice with the increase of the water content, NCs become smaller and side branching is prevented. Scale bar = 50 nm

Testing different alcohols (1-DDOL, 1,2-DDOL, 1,2-HDDOL, and 1,12-DDDOL) showed that the aliphatic chain length did not have evident influence on the NC growth, while the number of alcohol groups and their position just slightly modified the branch thickness and density (Figure S4). For instance, 1,12-DDDOL promoted more densely packed branched structures when compared with 1-DDOL or 1,2- HDDOL.

To enable their use in quasi-homogeneous catalysis reactions of in biomedical applications, and to facilitate their posterior assembly, ceria NCs produced in a non-polar organic solvent were rendered soluble in polar solvents and particularly water by means of Glm (see experimental details). Figure 6 shows the DLS spectra of quasi-spherical NCs and octapods before and after the ligand exchange and TEM images of the NCs supported on a carbon grid from a DMF solution (?).

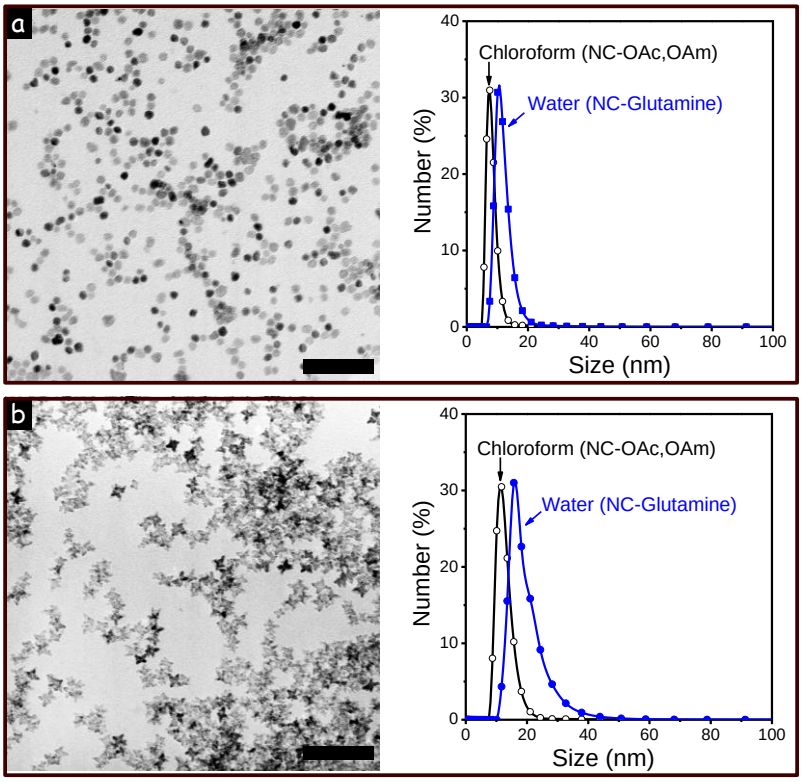

Figure 6. TEM micrograph and DLS spectra of ceria quasi-spherical NCs (a) and octapods (b) after ligand exchange. The DLS spectra of the NCs before the ligand exchange (in chloroform) is also shown as a reference. ("water" to be changed by proper solvent or spectra to be changed by the proper one!)

Additionally, ceria octapods were used to produce NC-based hydrogels and aerogels for their posterior use in catalytic applications. The gelation of a solution of amino-acid functionalized CeO_2 NCs in DMF and MQ-water was induced by PO. The hydrogel was dried under supercrititcal CO_2 to produce the corresponding aerogel. Figure 7 shows TEM images of drops of aerogels based on quasi-spherical NCs and octapods dried over a TEM grid.

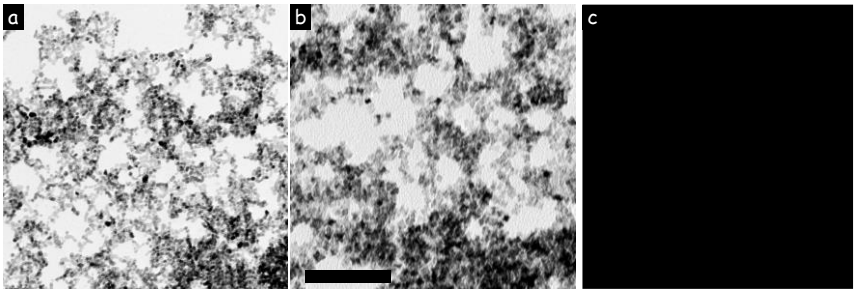

Figure 7. a,b) TEM micrograph of ceria aerogels produced from: a) quasi-spherical ceria NCs; b) ceria octapods. Scale bar (same for both images) = 50 nm. c) Photographs of the ceria NC-based hydrogel and aerogel (to be changed by the proper one!!).

Before characterizing their functional properties, ceria NCs were annealed at 400 ^{o}C for 4 hours under oxygen atmosphere to completely remove surface ligands. This temperature was selected on the basis that it allowed

to remove residual organics while conserving the NC morphologies. (Figure S12 and S13). Adsorption–desorption isotherm N_2 cycles were performed on the annealed samples showing type I physisorption isotherms characteristic of microporous materials for the quasi-spherical NCs and a distinctive IV type isotherm characteristic of mesoporous materials for all branched nanostructures (Figure 8a, Table 1).[74] The specific surface areas of the annealed samples were calculated using the Brunauer-Emmett-Teller (BET) model. As expected, branched structures were characterized by much higher surface areas, up to 212 m^2/g against 62.6 m^2/g for quasi-spheres. We associated these differences mainly to the different packing of each type of NC. This packing difference is also manifested in the much higher porosity obtained from the branched structures.

TPR profiles of the annealed samples showed two major features (Figure 8): In the range between 300-500 °C the reduction from Ce^{4+} to Ce^{3+} took place. This reduction occurred at lower temperatures at the NC surface compare with the bulk counterpart. The relative intensity between these two peaks in all the samples revealed a higher surface to volume ratio for the branched structures compared with the quasi-spherical, consistent with BET surface area results.[41,45] In the same direction, higher OSC values were also obtained for branched materials, reaching values up to 720 mmol O_2/g.

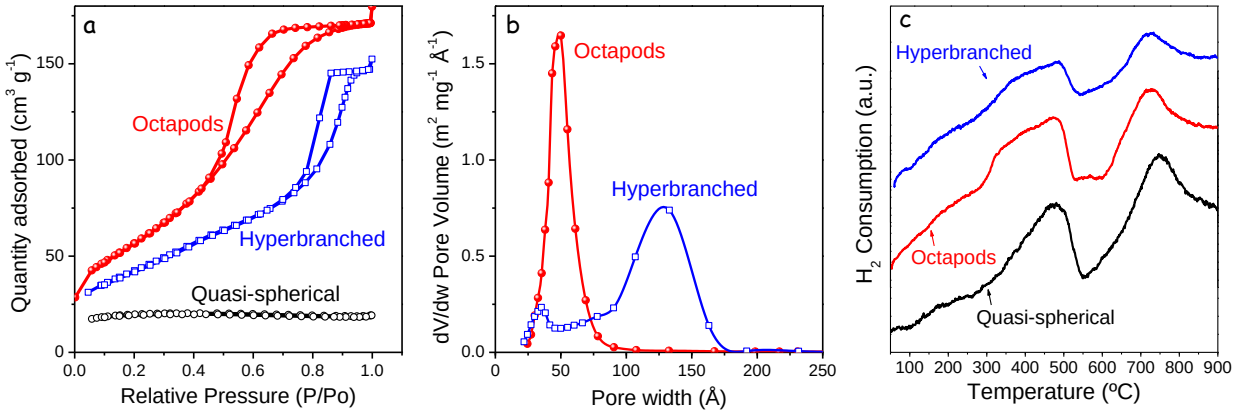

Figure 8: a) Adsorption/desorption isotherm cycles performed on quasi-spherical and branched ceria NCs. b) BJH pore size distributions. c) H_2 temperature-programmed reduction profiles. Samples were preheated at 90 °C for 15 min under a He flow (50 mL/min) before reducing them in a 12% vol H_2/Ar (50 mL/min) flow while increasing the temperature from room temperature up to 930 °C at a rate of 10 °C/min.

Table 1: Summary of the characterization performed on ceria isotropic clusters, thick-branched NCs, multi-branched NCs, and thin-branched NCs. Description of experiments is summarized in the experimental section.

CeO_2 NCs	BET Surface Area (m^2/g)	Pore Volume (cm^3/g)	Reduction at 823 K (x en CeO_x)[a]	OSC (µmol O/g)[b]
Quasi-spherical	62.6	0.03	1.81	488
Octapods	211.7	0.28	1.56	720
Hyperbranched	156.9	0.24	1.53	628

[a] Value of x in CeO_x as measured at 823 K from hydrogen consumption.
[b] Calculated from TGA in H_2 flow at 673 K.

CONCLUSIONS

Branched ceria NCs were synthesized by reacting cerium nitrate in the presence of OAm, OAc and alcohols. OAc was found to bond to the NC surface as an X-type ligand hindering NC growth in all crystallographic directions but less efficiently in the [111]. This effect was attributed to the lower OAc coverage of this facet due to the higher atomic compactness, lower coordination deficiency and reduced oxygen vacancy density of this surface. The preferential growth in this direction resulted in the formation of ceria octapods. The presence of alcohols strongly accelerated the nanocrystal growth through an esterification alcoholysis reaction, which resulted in larger NCs with higher aspect ratio arms and side branching. The concentration of water in the reaction mixture was found to play an import role in controlling this alcoholysis reaction. Ceria NCs were transferred to water through functionalization with amino acids and used to produce NC-based hydro- and aerogels. It was further demonstrated that branched NCs provided higher surface areas, porosities and OSC values when compared with quasi-spherical NCs.

REFERENCES

(1) Manna, L.; Milliron, D. J.; Meisel, A.; Scher, E. C.; Alivisatos, A. P. *Nat Mater* **2003**, *2*, 382.
(2) Li, H.; Kanaras, A. G.; Manna, L. *Accounts of Chemical Research* **2013**, *46*, 1387.
(3) Bierman, M. J.; Jin, S. *Energy & Environmental Science* **2009**, *2*, 1050.
(4) Ye, E.; Regulacio, M. D.; Zhang, S.-Y.; Loh, X. J.; Han, M.-Y. *Chemical Society Reviews* **2015**, *44*, 6001.
(5) Miszta, K.; de Graaf, J.; Bertoni, G.; Dorfs, D.; Brescia, R.; Marras, S.; Ceseracciu, L.; Cingolani, R.; van Roij, R.; Dijkstra, M.; Manna, L. *Nat Mater* **2011**, *10*, 872.
(6) Arciniegas, M. P.; Kim, M. R.; De Graaf, J.; Brescia, R.; Marras, S.; Miszta, K.; Dijkstra, M.; van Roij, R.; Manna, L. *Nano Letters* **2014**, *14*, 1056.
(7) Zhu, J.; Peng, H.; Chan, C. K.; Jarausch, K.; Zhang, X. F.; Cui, Y. *Nano Letters* **2007**, *7*, 1095.
(8) Yang, H.; Zhang, Y.; Hu, F.; Wang, Q. *Nano Letters* **2015**, *15*, 7616.
(9) Jiang, X.; Tian, B.; Xiang, J.; Qian, F.; Zheng, G.; Wang, H.; Mai, L.; Lieber, C. M. *Proceedings of the National Academy of Sciences* **2011**, *108*, 12212.
(10) Teng, X.; Liang, X.; Maksimuk, S.; Yang, H. *Small* **2006**, *2*, 249.
(11) Zhao, Z.; Zhou, Z.; Bao, J.; Wang, Z.; Hu, J.; Chi, X.; Ni, K.; Wang, R.; Chen, X.; Chen, Z.; Gao, J. *Nat Commun* **2013**, *4*.
(12) Rodríguez-Lorenzo, L.; de la Rica, R.; Álvarez-Puebla, R. A.; Liz-Marzán, L. M.; Stevens, M. M. *Nat Mater* **2012**, *11*, 604.
(13) Lim, B.; Xia, Y. *Angewandte Chemie International Edition* **2011**, *50*, 76.
(14) Guoqiang, X.; Minghui, S.; Kazuo, F.; Akihisa, I. In *Key Engineering Materials, Volume 1*; Apple Academic Press: 2014, p 185.
(15) Milliron, D. J.; Hughes, S. M.; Cui, Y.; Manna, L.; Li, J.; Wang, L.-W.; Paul Alivisatos, A. *Nature* **2004**, *430*, 190.
(16) Weiner, R. G.; Skrabalak, S. E. *Angewandte Chemie* **2015**, *127*, 1197.
(17) Stearns, L. A.; Chhabra, R.; Sharma, J.; Liu, Y.; Petuskey, W. T.; Yan, H.; Chaput, J. C. *Angewandte Chemie International Edition* **2009**, *48*, 8494.
(18) Sanz-Ortiz, M. N.; Sentosun, K.; Bals, S.; Liz-Marzán, L. M. *ACS Nano* **2015**, *9*, 10489.
(19) Ma, L.; Wang, C.; Gong, M.; Liao, L.; Long, R.; Wang, J.; Wu, D.; Zhong, W.; Kim, M. J.; Chen, Y.; Xie, Y.; Xiong, Y. *ACS Nano* **2012**, *6*, 9797.
(20) Tang, J.; Alivisatos, A. P. *Nano Letters* **2006**, *6*, 2701.
(21) Jun, Y.-w.; Chung, H.-W.; Jang, J.-t.; Cheon, J. *Journal of Materials Chemistry* **2011**, *21*, 10283.
(22) Fiore, A.; Mastria, R.; Lupo, M. G.; Lanzani, G.; Giannini, C.; Carlino, E.; Morello, G.; De Giorgi, M.; Li, Y.; Cingolani, R.; Manna, L. *Journal of the American Chemical Society* **2009**, *131*, 2274.

(23) Deka, S.; Miszta, K.; Dorfs, D.; Genovese, A.; Bertoni, G.; Manna, L. *Nano Letters* **2010**, *10*, 3770.
(24) Cheong, S.; Watt, J.; Ingham, B.; Toney, M. F.; Tilley, R. D. *Journal of the American Chemical Society* **2009**, *131*, 14590.
(25) Zhao, R.; Fu, G.; Zhou, T.; Chen, Y.; Zhu, X.; Tang, Y.; Lu, T. *Nanoscale* **2014**, *6*, 2776.
(26) Li, Y.; Ding, W.; Li, M.; Xia, H.; Wang, D.; Tao, X. *Journal of Materials Chemistry A* **2015**, *3*, 368.
(27) Lim, B.; Lu, X.; Jiang, M.; Camargo, P. H. C.; Cho, E. C.; Lee, E. P.; Xia, Y. *Nano Letters* **2008**, *8*, 4043.
(28) Raju, M.; van Duin, A. C. T.; Fichthorn, K. A. *Nano Letters* **2014**, *14*, 1836.
(29) Boneschanscher, M. P.; Evers, W. H.; Geuchies, J. J.; Altantzis, T.; Goris, B.; Rabouw, F. T.; van Rossum, S. A. P.; van der Zant, H. S. J.; Siebbeles, L. D. A.; Van Tendeloo, G.; Swart, I.; Hilhorst, J.; Petukhov, A. V.; Bals, S.; Vanmaekelbergh, D. *Science* **2014**, *344*, 1377.
(30) Sans, V.; Glatzel, S.; Douglas, F. J.; Maclaren, D. A.; Lapkin, A.; Cronin, L. *Chemical Science* **2014**, *5*, 1153.
(31) Tsai, Y.-H.; Chanda, K.; Chu, Y.-T.; Chiu, C.-Y.; Huang, M. H. *Nanoscale* **2014**, *6*, 8704.
(32) Sun, C.; Li, H.; Chen, L. *Energy & Environmental Science* **2012**, *5*, 8475.
(33) Zhang, Q.; Uchaker, E.; Candelaria, S. L.; Cao, G. *Chemical Society Reviews* **2013**, *42*, 3127.
(34) Walkey, C.; Das, S.; Seal, S.; Erlichman, J.; Heckman, K.; Ghibelli, L.; Traversa, E.; McGinnis, J. F.; Self, W. T. *Environmental Science: Nano* **2015**, *2*, 33.
(35) Krishnan, M.; Nalaskowski, J. W.; Cook, L. M. *Chemical Reviews* **2010**, *110*, 178.
(36) Trovarelli, A. *Catalysis Reviews* **1996**, *38*, 439.
(37) Campbell, C. T.; Peden, C. H. F. *Science* **2005**, *309*, 713.
(38) Esch, F.; Fabris, S.; Zhou, L.; Montini, T.; Africh, C.; Fornasiero, P.; Comelli, G.; Rosei, R. *Science* **2005**, *309*, 752.
(39) Mullins, D.; Albrecht, P.; Calaza, F. *Top Catal* **2013**, *56*, 1345.
(40) Sun, C.; Xue, D. *Physical Chemistry Chemical Physics* **2013**, *15*, 14414.
(41) Aneggi, E.; Wiater, D.; de Leitenburg, C.; Llorca, J.; Trovarelli, A. *ACS Catalysis* **2014**, *4*, 172.
(42) Hsiao, W.-I.; Lin, Y.-S.; Chen, Y.-C.; Lee, C.-S. *Chemical Physics Letters* **2007**, *441*, 294.
(43) Nolan, M.; Parker, S. C.; Watson, G. W. *Surface Science* **2005**, *595*, 223.
(44) Conesa, J. *Surface Science* **1995**, *339*, 337.
(45) Vilé, G.; Colussi, S.; Krumeich, F.; Trovarelli, A.; Pérez-Ramírez, J. *Angewandte Chemie International Edition* **2014**, *53*, 12069.
(46) Mann, A. K. P.; Wu, Z.; Overbury, S. H. In *Catalysis by Materials with Well-Defined Structures*; Overbury, Z. W. H., Ed.; Elsevier: Amsterdam, 2015, p 71.
(47) Lei, W.; Zhang, T.; Gu, L.; Liu, P.; Rodriguez, J. A.; Liu, G.; Liu, M. *ACS Catalysis* **2015**, *5*, 4385.
(48) Jiang, D.; Wang, W.; Zhang, L.; Zheng, Y.; Wang, Z. *ACS Catalysis* **2015**, *5*, 4851.
(49) Mann, A. K. P.; Wu, Z.; Calaza, F. C.; Overbury, S. H. *ACS Catalysis* **2014**, *4*, 2437.
(50) Wu, Z.; Li, M.; Overbury, S. H. *Journal of Catalysis* **2012**, *285*, 61.
(51) Sayle, D. C.; Maicaneanu, S. A.; Watson, G. W. *Journal of the American Chemical Society* **2002**, *124*, 11429.
(52) Si, R.; Flytzani-Stephanopoulos, M. *Angewandte Chemie International Edition* **2008**, *47*, 2884.
(53) Zabilskiy, M.; Djinović, P.; Tchernychova, E.; Tkachenko, O. P.; Kustov, L. M.; Pintar, A. *ACS Catalysis* **2015**, *5*, 5357.
(54) Soler, L.; Casanovas, A.; Urrich, A.; Angurell, I.; Llorca, J. *Applied Catalysis B: Environmental* **2016**, *197*, 47.
(55) Carrettin, S.; Concepción, P.; Corma, A.; López Nieto, J. M.; Puntes, V. F. *Angewandte Chemie International Edition* **2004**, *43*, 2538.
(56) Yu, T.; Joo, J.; Park, Y. I.; Hyeon, T. *Angewandte Chemie International Edition* **2005**, *44*, 7411.
(57) Mai, H.-X.; Sun, L.-D.; Zhang, Y.-W.; Si, R.; Feng, W.; Zhang, H.-P.; Liu, H.-C.; Yan, C.-H. *The Journal of Physical Chemistry B* **2005**, *109*, 24380.
(58) Yang, S.; Gao, L. *Journal of the American Chemical Society* **2006**, *128*, 9330.
(59) Pan, C.; Zhang, D.; Shi, L.; Fang, J. *European Journal of Inorganic Chemistry* **2008**, *2008*, 2429.

(60) Wang, D.; Kang, Y.; Doan-Nguyen, V.; Chen, J.; Küngas, R.; Wieder, N. L.; Bakhmutsky, K.; Gorte, R. J.; Murray, C. B. *Angewandte Chemie International Edition* **2011**, *50*, 4378.
(61) Li, P.; Zhou, Y.; Zhao, Z.; Xu, Q.; Wang, X.; Xiao, M.; Zou, Z. *Journal of the American Chemical Society* **2015**, *137*, 9547.
(62) Lee, S. S.; Song, W.; Cho, M.; Puppala, H. L.; Nguyen, P.; Zhu, H.; Segatori, L.; Colvin, V. L. *ACS Nano* **2013**, *7*, 9693.
(63) Sridaeng, D.; Limsirinawa, A.; Sirojpornphasut, P.; Chawiwannakorn, S.; Chantarasiri, N. *Journal of Applied Polymer Science* **2015**, *132*, n/a.
(64) Jun, Y.-w.; Choi, J.-s.; Cheon, J. *Angewandte Chemie International Edition* **2006**, *45*, 3414.
(65) Zhang, J.; Ohara, S.; Umetsu, M.; Naka, T.; Hatakeyama, Y.; Adschiri, T. *Advanced Materials* **2007**, *19*, 203.
(66) Zhang, Q.; Xie, J.; Yu, Y.; Lee, J. Y. *Nanoscale* **2010**, *2*, 1962.
(67) Sun, S.; Zeng, H. *Journal of the American Chemical Society* **2002**, *124*, 8204.
(68) Yang, J.; Sargent, E.; Kelley, S.; Ying, J. Y. *Nat Mater* **2009**, *8*, 683.
(69) Deori, K.; Gupta, D.; Saha, B.; Deka, S. *ACS Catalysis* **2014**, *4*, 10.
(70) Buonsanti, R.; Llordes, A.; Aloni, S.; Helms, B. A.; Milliron, D. J. *Nano Letters* **2011**, *11*, 4706.
(71) Zhong, X.; Feng, Y.; Zhang, Y.; Lieberwirth, I.; Knoll, W. *Small* **2007**, *3*, 1194.
(72) Lee, S. S.; Zhu, H.; Contreras, E. Q.; Prakash, A.; Puppala, H. L.; Colvin, V. L. *Chemistry of Materials* **2012**, *24*, 424.
(73) Ould-Ely, T.; Prieto-Centurion, D.; Kumar, A.; Guo, W.; Knowles, W. V.; Asokan, S.; Wong, M. S.; Rusakova, I.; Lüttge, A.; Whitmire, K. H. *Chemistry of Materials* **2006**, *18*, 1821.
(74) Sing, K. S. W.; Everett, D. H.; Haul, R. A. W.; Moscou, L.; Pierotti, R. A.; Rouquerol, J.; Siemieniewska, T. *Pure and Applied Chemistry* **1985**, *57*, 603.